Emergence and Decay of Turbulence in Stirred Atomic Bose-Einstein Condensates

N. G. Parker and C. S. Adams

Department of Physics, University of Durham, South Road, Durham DH1 3LE, United Kingdom
(Received 30 May 2005; published 29 September 2005)

We show that a "weak" elliptical deformation of an atomic Bose-Einstein condensate rotating at close to the quadrupole instability frequency leads to turbulence with a Kolmogorov energy spectrum. The turbulent state is produced by energy transfer to condensate fragments that are ejected by the quadrupole instability. This energy transfer is driven by breaking the twofold rotational symmetry of the condensate. Subsequently, vortex-sound interactions damp the turbulent state leading to the crystallization of a vortex lattice.

Two-dimensional (2D) turbulence has been explored in diverse areas such as soap films [1], magnetohydroynamics [2], and meteorology (see [3] and references therein), and can often display additional features not present in 3D [4]. However, the complexities of real fluids mean that the theoretical predictions are often at odds with observed spectra. In this regard there may be some advantages in studying superfluids where the absence of viscosity and the quantization of vorticity can simplify the theoretical picture. For example, superfluid turbulence in liquid helium [5] is found to exhibit analogous features to classical turbulence, in particular, a Kolmogorov energy spectrum [6]. Even more amenable to theoretical description are atomic Bose-Einstein condensates (BECs) [7]. In addition, atomic BECs allow the flexibility of studying the transition between 2D and 3D turbulence.

Recent experiments on atomic BECs have generated vortex lattices by thermodynamically condensing a rotating thermal cloud [8] and mechanical rotation of the condensate in an anharmonic trap [9–11]. In the latter case, a quadrupolar collective mode of the condensate is excited. A dynamical instability [12,13] leads to the nucleation of vortices, which subsequently crystallize into a lattice configuration. The time scale for vortex lattice formation has been shown to be insensitive to temperature [11,14], suggesting that the process is a purely dynamical effect. The formation of the lattice has been simulated using the time-dependent Gross-Pitaevskii equation (GPE) [15–18] (although [15,16] required the inclusion of damping effects). However, questions remain over the dynamics involved, for example, how the dynamical instability seeds vortex nucleation, what is the damping mechanism leading to the crystallization of the lattice, and the role of dimensionality in the process.

In this Letter, we present evidence that 2D turbulence is a key feature of current experiments on vortex lattice formation in atomic BECs. In particular, we show that the route to lattice formation can be divided into four distinct stages, as illustrated in Fig. 1. These stages are as follows.

Fragmentation.—The quadrupolar mode breaks down, ejecting energetic atoms to form an outer cloud.

Symmetry breaking.—The twofold rotational symmetry of the system is broken in a macroscopic manner, allowing the rotation to couple to additional modes, thereby injecting energy rapidly into the system.

Turbulence.—A turbulent cloud containing vortices and high energy density fluctuations (sound field) is formed, with a Kolmogorov energy spectrum.

Crystallization.—The loss of energy at short length scales coupled with the vortex-sound interactions [19,20] allow the system to relax into an ordered lattice.

Our analysis is based on the classical field method whereby the GPE is used to describe both the condensate mean-field ψ and fluctuations [21]. Fluctuations in the initial state speed up the evolution through the four stages but do not change the qualitative behavior. For illustrative purposes we use an initial state without excitations. The rotating trap strongly polarizes the dynamics along the z axis, such that 2D dynamics in the rotating plane dominate the system. Indeed, we have verified that the same results are obtained in the flattened, quasi-2D geometry by solving the 3D GPE. We therefore proceed in the 2D limit by
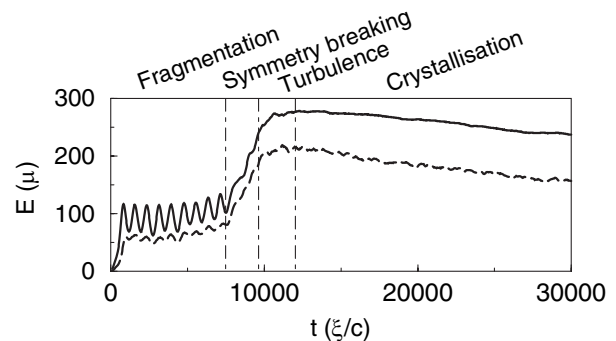

FIG. 1. The condensate energy (black line) and energy of the outer cloud (dashed line), defined as the region with $n < 0.2n_0$, as a function of time, with a trap rotation frequency $\Omega = 0.77\omega_r$. The four distinct stages of the evolution (see text) are indicated.

solving the computationally advantageous 2D GPE, as in our previous work [19]. We have performed simulations for a range of condensate sizes, and various grid and box sizes, and find the same qualitative results throughout. We characterize the state of the system in terms of the energy. The instantaneous condensate energy at time t is given by the GPE energy functional,

$$E(t) = \int \left[-\frac{\hbar^2}{2m} |\nabla\psi(t)|^2 + V(t)|\psi(t)|^2 + \frac{g}{2}|\psi(t)|^4 \right] dx\,dy,$$

(1)

and from this we subtract the corresponding energy of the initial state. Here V is the external potential, m is the atomic mass, and $g = 4\pi\hbar^2 Na/m$, where N is the number of atoms and a is the s-wave scattering length.

To apply a rotation we use a "weakly" elliptical potential similar to the experiments [9,11] (the stirring potential used in Ref. [10] is strongly anharmonic). The potential is written in the laboratory frame (rather than the rotating frame [15,16,18]) as

$$V(t) = \frac{1}{2} m\omega_r^2 [(x^2 + y^2) + \varepsilon(x\cos\Omega t - y\sin\Omega t)^2$$
$$- \varepsilon(x\sin\Omega t + y\cos\Omega t)^2].$$

(2)

The first term represents the static harmonic trap with transverse frequency ω_r. The second and third terms represent the elliptical trap perturbation rotating at frequency Ω. The trap ellipticity is taken to be $\varepsilon = 0.025$ [9].

Our units of length, time, and energy are the healing length $\xi = \hbar/\sqrt{m\mu}$, (ξ/c), and the chemical potential $\mu = n_0 g$. Here $c = \sqrt{\mu/m}$ is the Bogoliubov speed of sound, and n_0 is the peak condensate density. For a typical ^{87}Rb BEC, the units of distance and time correspond to $\xi \sim 0.3\ \mu$m and $(\xi/c) \sim 10^{-4}$ s, respectively.

Fragmentation.—At $t = 0$, the rotation is turned on. The rotating trap couples energy into the condensate by exciting a quadrupolar shape oscillation, while the axes of the quadrupole rotate at the trap rotation frequency Ω. This excitation mimics rotation yet the system remains irrotational. In the radially symmetric system, the quadrupole mode is predicted to have a resonant frequency at $\Omega = \omega_r/\sqrt{2}$ [22], but this is shifted slightly by the ellipticity. Away from the resonance the quadrupole oscillations have reduced amplitude and are stable. The condensate cycles between the initial circular state and a higher energy elongated state, but over a complete cycle there is no *net* increase in energy. Such quadrupole oscillations have been observed experimentally [23].

The condensate is predicted to be dynamically unstable at the quadrupole resonant frequency [13]. The instability arises because the amplitude of the mode becomes so large that the quadrupolar irrotational flow can no longer be supported. As the condensate relaxes from the point of maximum elongation, the fluid cannot adjust sufficiently quickly back towards the center of the trap. This results in

the shedding of fluid from the ends of the condensate forming low density tails and giving the condensate a spiral shape [Fig. 2(a)(ii)]. The ejected material collapses back onto the condensate edge, forming phase dislocations with the main condensate. This generates surface waves and "ghost" vortices [15,17]. An outer, low density ($\sim 0.1n_0$) cloud is formed [Fig. 2(a)(iii)]. After the condensate has shed material [Fig. 2(b), solid line], its energy no longer decreases to the initial value—energy has been transferred irreversibly into the condensate. We monitor the relative evolution of the outer, low density cloud and the inner, high density condensate by defining the outer cloud to be where the density is less than a certain value, taken here to be $0.2n_0$. The injected energy goes primarily into the outer cloud [Fig. 2(b), dashed line]. Note that, although the energy of the inner and outer clouds are comparable, the outer cloud contains only about 10% of the total atoms, and therefore the average energy per atom is considerably higher. Subsequently, the inner cloud continues to undergo quadrupole oscillations and eject small fragments, as indicated by the energy curves shown in Fig. 2(b). Also, the outer cloud develops more structure at short length scales [Fig. 2(a)(iv)].

For the parameters employed here, we observe the fragmentation of the cloud (and ultimately the formation of a vortex lattice) for rotation frequencies in the range $0.72 < \Omega/\omega_r < 0.78$, which is in reasonable agreement with the experimental results of Madison *et al.* [9]. Outside this range the quadrupole mode is stable, and the width of the unstable region increases with the trap ellipticity ε, which is consistent with the experimental observations of Hodby *et al.* [11].

Symmetry breaking.—The condensate and potential have a twofold rotational symmetry [clearly visible in Fig. 2(a)]. In the experiments [9,11] this symmetry is absent. Eventually in the simulations, an asymmetry grows out of the numerical noise generated by modeling a rota-
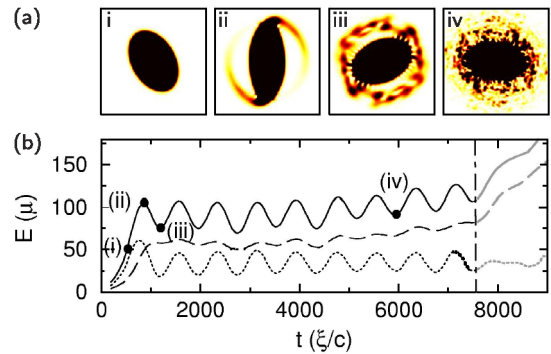

FIG. 2 (color online). Fragmentation: (a) Snapshots of the condensate density in the range $(0–0.05n_0)$ at times $t \approx$ (i) 400, (ii) 800, (iii) 1200, and (iv) 6000 (ξ/c). Each plot represents a region $[-30, 30]\xi \times [-30, 30]\xi$ (while the numerical box is much larger). Dark represents high density. (b) Total condensate energy (solid line), energy of inner cloud (dotted line), and energy of outer cloud (dashed line).

tion using a static square grid. We characterize this asymmetry in terms of an asymmetry parameter defined as

$$\sigma = \frac{\int [|\psi(x, y)|^2 - |\psi(-x, -y)|^2] dx dy}{\int |\psi(x, y)|^2 dx dy}. \quad (3)$$

This asymmetry parameter [Fig. 3(b), solid line] grows exponentially over time. When it reaches macroscopic levels ($\sigma \sim 0.1$), we enter a symmetry-breaking phase at $t \sim 8000(\xi/c)$. From then on, additional modes can be excited, and energy is rapidly coupled into the system [Fig. 3(a), solid line]. This energy predominantly excites the outer, low density cloud, as shown in Fig. 1 (dashed line). The condensate density and phase during this stage are shown in Figs. 3(c) and 3(d). The original twofold rotational symmetry is now clearly broken. Towards the end of this stage the outer cloud strongly couples to, and merges with, the inner condensate. Energy and angular momentum become transferred to the inner cloud, the quadrupole mode finally breaks down, and vortices become nucleated in the higher density regions.

In experiments, symmetry breaking will occur due to, for example, the thermal cloud, quantum fluctuations, trap imperfections, and fluctuating fields. We model the effect by allowing the trap center to randomly jump, or jitter, within a region $[-\gamma, +\gamma] \times [-\gamma, +\gamma]$. Figures 3(a) and 3(b) show the results for trap jitters of $\gamma = 0.0001$ (dashed line) and 0.1 (dotted line). We observe the same *qualitative* behavior as in the absence of the jitter, although the macroscopic symmetry breaking occurs earlier when jitter is added. Even for an extremely small jitter ($\gamma = 0.0001\xi$, 3 orders of magnitude smaller than the grid size) the effect is significant, thereby demonstrating the importance of symmetry. Symmetry-breaking allows vortices to enter the condensate one by one, rather than in opposing pairs [15], which reduces the threshold energy for vortex nucleation.

Turbulence.—Following the injection of energy into the condensate during the symmetry-breaking stage, a highly excited and energetic condensate containing randomly positioned vortices is formed, as shown in Figs. 4(a) and 4(b). We analyze this stage of the evolution by calculating the energy spectrum, shown in Fig. 4(c). During the turbulent phase the system closely follows a Kolmogorov energy spectrum $E(k) \propto k^{-5/3}$ over a range of k values, as shown in Fig. 4(c) (bold line) for $t = 11\,000(\xi/c)$. Such behavior is a key signature of classical turbulence and also occurs in models of superfluid turbulence [6]. The departure from a $k^{-5/3}$ law occurs at an upper bound of $k \approx 2(2\pi/\xi)$, corresponding to the characteristic length scale of vortex-sound interactions [20], and a lower bound of $k \approx 0.3(2\pi/\xi)$, corresponding to the size of the condensate. An additional feature of 2D classical turbulence is that the spectrum is predicted to show k^{-3} behavior following the $k^{-5/3}$ region [4]. However, we observe a k^{-6} dependence in this range. The power spectrum in the fragmentation stage [Fig. 4(a), intermediate gray] and the succeeding crystallization stage [Fig. 4(a), light gray] do not show a $k^{-5/3}$ behavior.

Crystallization.—The turbulent state contains a dense sound field and vortices. In previous work we have shown how vortices can both radiate and absorb sound waves in a Bose-Einstein condensate [19,20]. We propose that this vortex-sound interaction enables the randomly positioned vortices in our rotating condensate to crystallize into a lattice.

To demonstrate the transfer of energy from the sound field (density fluctuations) to the vortices, we divide the energy into a component due to the vortices E_V and a component due to the sound field E_S. To approximate E_V at a particular time we take the real-time vortex distribution, and impose this on a separate state with the same potential and number of particles. By propagating the GPE in imaginary time, we obtain the lowest energy state with this vortex distribution but without sound. The energy of this state is E_V. The sound energy is then defined as
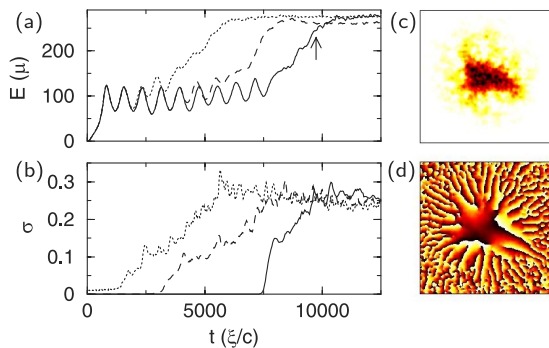

FIG. 3 (color online). Symmetry breaking: Evolution of (a) total condensate energy and (b) condensate asymmetry parameter for no trap jitter (solid line), and trap jitters of $\gamma = 0.0001$ (dashed line) and $\gamma = 0.1$ (dotted line). (c)–(d) Snapshots of the total condensate density and phase, respectively, during the symmetry-breaking stage at $t = 9600(\xi/c)$ in the absence of trap jitter.
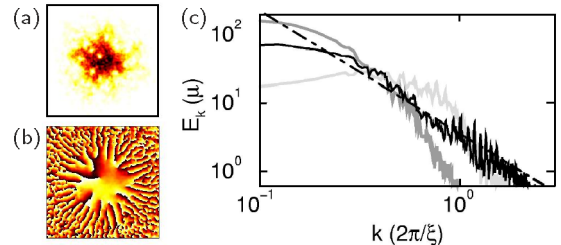

FIG. 4 (color online). Turbulence: Snapshots of the turbulent (a) condensate density and (b) phase at $t = 11\,000(\xi/c)$. The vortices are characterized by a node in the density and an azimuthal phase change of 2π. (c) Energy spectrum in k space during (i) the turbulent stage at $t = 11\,000(\xi/c)$ (bold line); (ii) fragmentation at $t = 8000(\xi/c)$ (intermediate gray line); and crystallization at $t = 20\,000(\xi/c)$ (light gray line). The turbulent Kolmorogov behavior $E_k \propto k^{-5/3}$ is indicated (dot-dashed line).
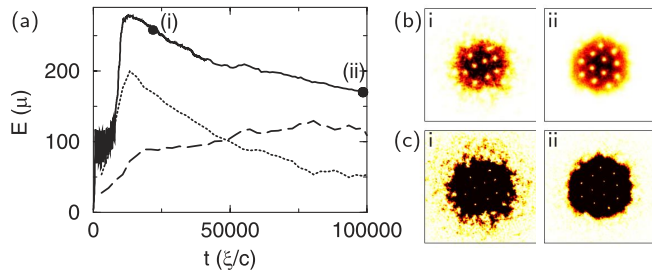
FIG. 5 (color online). Crystallization: (a) Total condensate energy (solid line), sound energy (dotted line), and vortex energy (dashed line). Snapshots of the (a) total condensate density (0–n_0) and (b) low density (0–$0.05n_0$) at times (i) $20\,000$ and (ii) $100\,000(\xi/c)$.

$E_S = E - E_V$. During the fragmentation, symmetry-breaking, and turbulent stages, both sound energy [Fig. 5(a), dotted line] and vortex energy [Fig. 5(a), dashed line] are fed into the system. At the start of the crystallization phase the sound energy is considerably higher than the vortex energy. However, as time progresses the sound energy decreases with this energy being transferred to the vortices. Figures 5(b) and 5(c) show the condensate density at the beginning and towards the end of the crystallization phase. We see that the conversion of sound energy into vortex energy is associated with the ordering of the vortices from a disordered distribution to a lattice configuration and a smoothing of the condensate profile [Fig. 5(b)]. Furthermore, the outer cloud shrinks [Fig. 5(c)]. By the time $t = 100\,000(\xi/c)$ the vortex energy is substantially greater than the sound energy. At this point we observe a well-ordered vortex lattice.

In our simulations, the finite grid size sets a maximum value in momentum space, with higher k modes having zero occupation [21]. We have imposed reduced values of the momentum cutoff and consistently observe lattice formation, with no marked effect on its time scale. This further supports the idea that the vortex lattice formation is independent of thermal effects.

In the vortex lattice experiments [9,11], the lattices are observed after up to 1 s of trap rotation. In our simulation, a noisy lattice has formed by $t \sim 2$ s [Fig. 5(b)(i)], while it takes several more seconds for the vortices to settle into a clean lattice. However, as shown in Fig. 3, the time scale of the fragmentation stage is sensitive to the degree of symmetry-breaking effects present in the system, as well as the trap rotation frequency and ellipticity. One would therefore expect that in a real system, with all its inherent imperfections, the time scale for this stage will be reduced.

Note that if the rotation is terminated before the peak energy has been coupled into the system, the lattice still forms, albeit at a lower energy. This allows control over the ultimate number of vortices in the lattice.

In summary, we have shown that "stirring" atomic condensates generates turbulence. We verify that a $k^{-5/3}$ power law is observed for two-dimensional superfluid turbulence. The turbulent state subsequently evolves into a vortex lattice by vortex-sound interactions. Future work will focus on turbulence in spinor systems and the effect of dimensionality on the turbulence spectrum.

[1] Y. Couder, J. M. Chomaz, and M. Rabaud, Physica (Amsterdam) **37D**, 384 (1989); M. Gharib and P. Derango, Physica (Amsterdam) **37D**, 406 (1989).

[2] O. Cardoso, D. Marteau, and P. Tabeling, Phys. Rev. E **49**, 454 (1994).

[3] K. S. Smith, J. Atmos. Sci. **61**, 937 (2004).

[4] R. H. Kraichnan, Phys. Fluids **10**, 1417 (1967); C. E. Leith, Phys. Fluids **11**, 671 (1968); G. K. Batchelor, Phys. Fluids (Suppl.) II **12**, 233 (1969).

[5] *Quantized Vortex Dynamics and Superfluid Turbulence*, edited by C. F. Barenghi, R. J. Donnelly, and W. F. Vinen (Springer, Berlin, 2001).

[6] C. Nore, M. Abid, and M. E. Brachet, Phys. Rev. Lett. **78**, 3896 (1997); T. Araki, M. Tsubota, and S. K. Nemirovskii, Phys. Rev. Lett. **89**, 145301 (2002); M. Kobayashi and M. Tsubota, Phys. Rev. Lett. **94**, 065302 (2005).

[7] F. Dalfovo, S. Giorgini, L. P. Pitaevskii, and S. Stringari, Rev. Mod. Phys. **71**, 463 (1999).

[8] P. C. Haljan, I. Coddington, P. Engels, and E. A. Cornell, Phys. Rev. Lett. **87**, 210403 (2001).

[9] K. W. Madison, F. Chevy, W. Wohlleben, and J. Dalibard, Phys. Rev. Lett. **84**, 806 (2000).

[10] J. R. Abo-Shaeer, C. Raman, J. M. Vogels, and W. Ketterle, Science **292**, 476 (2001).

[11] E. Hodby *et al.*, Phys. Rev. Lett. **88**, 010405 (2002).

[12] K. W. Madison, F. Chevy, V. Bretin, and J. Dalibard, Phys. Rev. Lett. **86**, 4443 (2001).

[13] S. Sinha and Y. Castin, Phys. Rev. Lett. **87**, 190402 (2001).

[14] J. R. Abo-Shaeer, C. Raman, and W. Ketterle, Phys. Rev. Lett. **88**, 070409 (2002).

[15] M. Tsubota, K. Kasamatsu, and M. Ueda, Phys. Rev. A **65**, 023603 (2002); K. Kasamatsu, M. Tsubota, and M. Ueda, Phys. Rev. A **67**, 033610 (2003).

[16] A. A. Penckwitt, R. J. Ballagh, and C. W. Gardiner, Phys. Rev. Lett. **89**, 260402 (2002).

[17] E. Lundh, J. P. Martikainen, and K. A. Suominen, Phys. Rev. A **67**, 063604 (2003).

[18] C. Lobo, A. Sinatra, and Y. Castin, Phys. Rev. Lett. **92**, 020403 (2004).

[19] N. G. Parker, N. P. Proukakis, C. F. Barenghi, and C. S. Adams, Phys. Rev. Lett. **92**, 160403 (2004).

[20] M. Leadbeater *et al.*, Phys. Rev. Lett. **86**, 1410 (2001).

[21] M. J. Davis, S. A. Morgan, and K. Burnett, Phys. Rev. Lett. **87**, 160402 (2001); K. Goral, M. Gajda, and K. Rzazewski, Opt. Express **8**, 92 (2001); A. A. Norrie, R. J. Ballagh, and C. W. Gardiner, Phys. Rev. Lett. **94**, 040401 (2005).

[22] S. Stringari, Phys. Rev. Lett. **77**, 2360 (1996).

[23] F. Chevy, K. W. Madison, and J. Dalibard, Phys. Rev. Lett. **85**, 2223 (2000); G. Hechenblaikner *et al.*, Phys. Rev. Lett. **88**, 070406 (2002).